

COL778: Principles of Autonomous Systems

Assignment 1

Harshit Goyal 2021MT10143

February 2025

Contents

1 State Estimation of 1D motion using Kalman Filters

1.1	Motion and Observation models
1.2	Kalman Filter Model
1.3	Uncertainty Bars for x_t^e
1.4	Varying $\sigma_x, \sigma_{\dot{x}}, \sigma_s$
1.5	Kalman Gain
1.6	Missing Observations

2 State Estimation of 3D motion using Kalman Filters

2.1	Motion and Observation models
2.2	Kalman Filter Model
2.3	Automated Referee
2.4	Varying noise parameters in Automated Referee
2.5	Uncertainty Ellipses on Trajectory
2.6	Base-Stations in 2D Kinematics

3 More insights after viva

Please find all html plots at [here](#).

1 State Estimation of 1D motion using Kalman Filters

1.1 Motion and Observation models

1. We run the Kalman update after every Δt time-step. The state $X_t \in \mathbb{R}^2$ denotes

$$X_t = \begin{bmatrix} x_t \\ \dot{x}_t \end{bmatrix}$$

2. The initial belief $X_0 \sim \mathcal{N}(0, 10^{-4}I_2)$. u_t is a scalar. The motion model is

$$X_{t+1} = A_t X_t + B_t u_t + \epsilon_t$$

where $A_t = \begin{bmatrix} 1 & \Delta t \\ 0 & 1 \end{bmatrix}$, $B_t = \begin{bmatrix} \frac{1}{2}\Delta t^2 \\ \Delta t \end{bmatrix}$, $\epsilon_t \sim \mathcal{N}(0, R_t)$

where $R_t = \begin{bmatrix} \sigma_x^2 & 0 \\ 0 & \sigma_{\dot{x}}^2 \end{bmatrix}$

3. The observations $Z_t \in \mathbb{R}$ are the noisy value of time taken for sound wave to start from $x = 0$, hit the train and come back. The observation model is

$$Z_t = C_t X_t + \delta_t$$

where $C_t = \begin{bmatrix} \frac{2}{v_{sound}} & 0 \end{bmatrix}$, $\delta_t \sim \mathcal{N}(0, \sigma_s^2)$

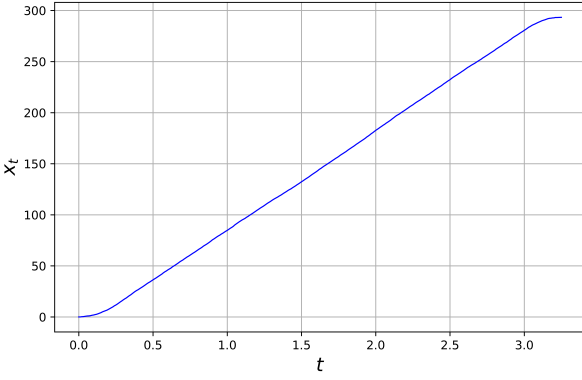


Figure 1: Ground truth x_t vs t

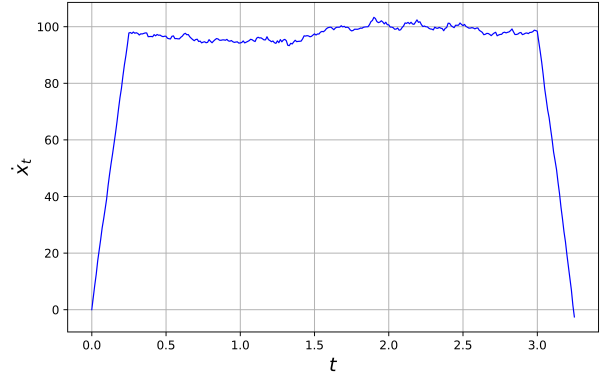


Figure 2: Ground truth \dot{x}_t vs t

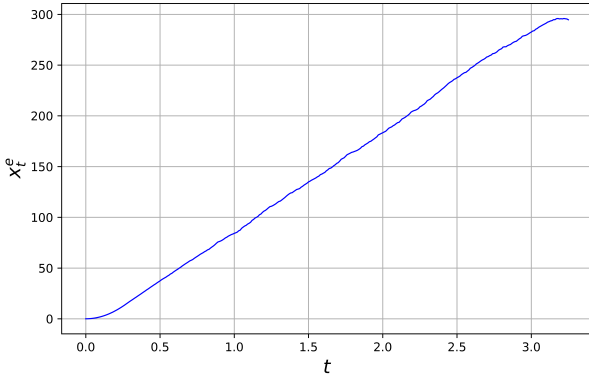


Figure 3: Estimation x_t^e vs t

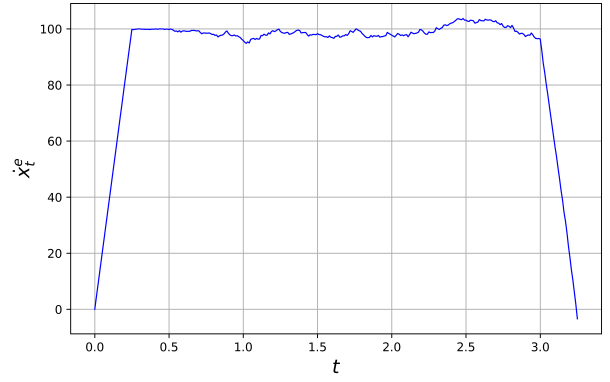


Figure 4: Estimation \dot{x}_t^e vs t

1.2 Kalman Filter Model

In [Kalman Filter Algorithm](#), $\mu_0 = [0 \ 0]^T$, $\Sigma_0 = 10^{-4}I_2$ is the initial belief. Values of A_t, B_t, R_t, C_t, Q_t have been given in [Motion and Observation models](#).

```

Algorithm Kalman_filter( $\mu_{t-1}, \Sigma_{t-1}, u_t, z_t$ )
Prediction Step
 $\bar{\mu}_t = A_t \mu_{t-1} + B_t u_t$ 
 $\bar{\Sigma}_t = A_t \Sigma_{t-1} A_t^T + R_t$ 
Update Step
 $K_t = \bar{\Sigma}_t C_t^T (C_t \bar{\Sigma}_t C_t^T + Q_t)^{-1}$ 
 $\mu_t = \bar{\mu}_t + K_t (z_t - C_t \bar{\mu}_t)$ 
 $\Sigma_t = (I - K_t C_t) \bar{\Sigma}_t$ 
return  $\mu_t, \Sigma_t$ 

```

Figure 5: Kalman Filter Algorithm

1.3 Uncertainty Bars for x_t^e

In [Figure 6](#) we see that the uncertainty bar is very thin initially, but it becomes wider later, possibly due to the error in action the model R_t that keeps getting added in each step. For most of the time, the one-standard-deviation uncertainty band contains the ground truth.

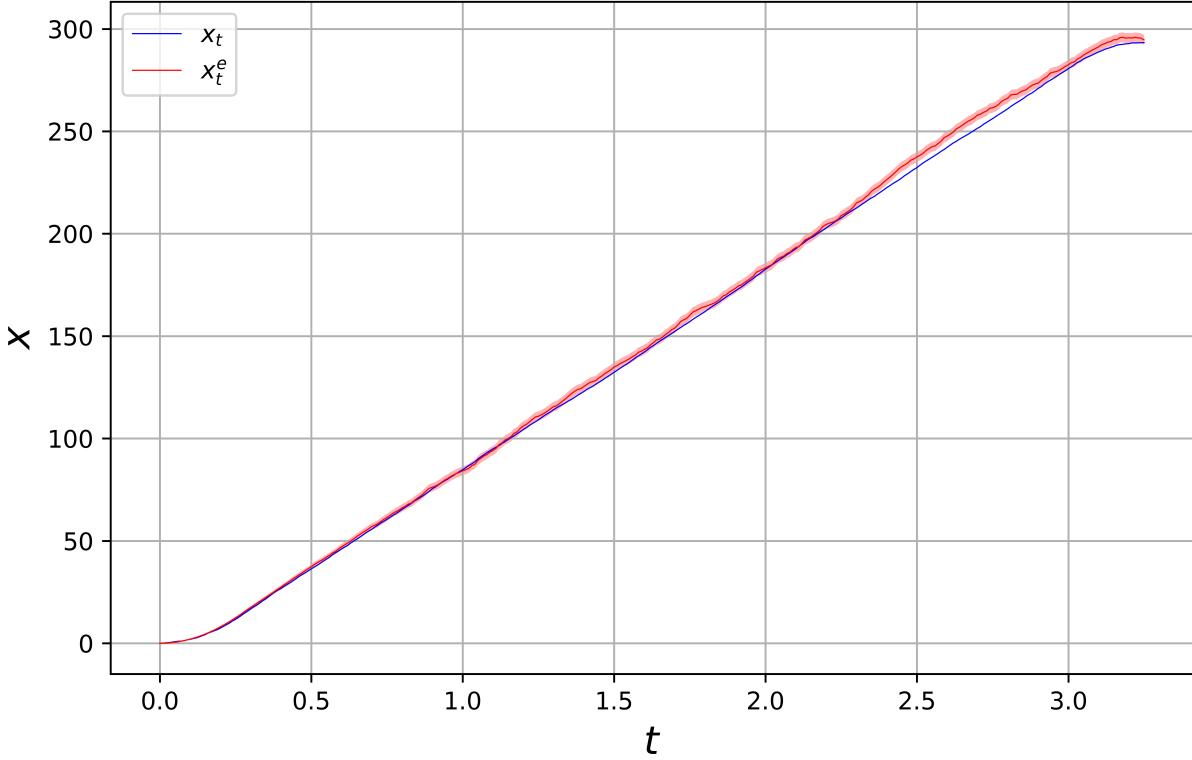
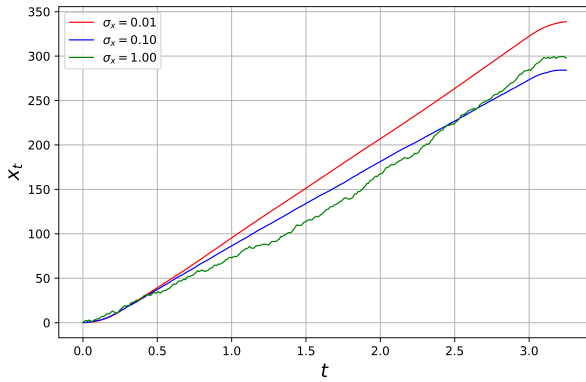


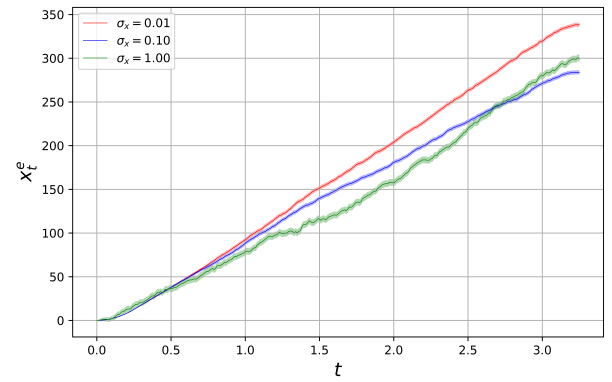
Figure 6: x_t and Uncertainty bar of x_t^e

1.4 Varying $\sigma_x, \sigma_{\dot{x}}, \sigma_s$

- In [Figure 7](#) The uncertainty band gets wider on increasing σ_x . Both ground truth and estimated trajectories are affected, as σ_x causes noise in the motion model.
- In [Figure 8](#), both ground truth and estimated trajectories with $\sigma_{\dot{x}} = 5.0$ are significantly different from those with lower $\sigma_{\dot{x}}$. This is because $\sigma_{\dot{x}}$ directly affects the noise in the motion model. The uncertainty band becomes wider, and there are many more fluctuations as $\sigma_{\dot{x}}$ is increased.
- [Figure 9](#) shows, on changing σ_s there's nearly no variation in x_t as the ground truth does not use observations. The difference is only due to the random noise in the motion model. In x_t^e , the uncertainty band clearly becomes wider as σ_s increases. As observation is the only part in Kalman Filter where the belief variance reduces. The trajectories themselves, however, are not very different (varying σ_s) compared to the earlier parts (causing noise in the motion model).

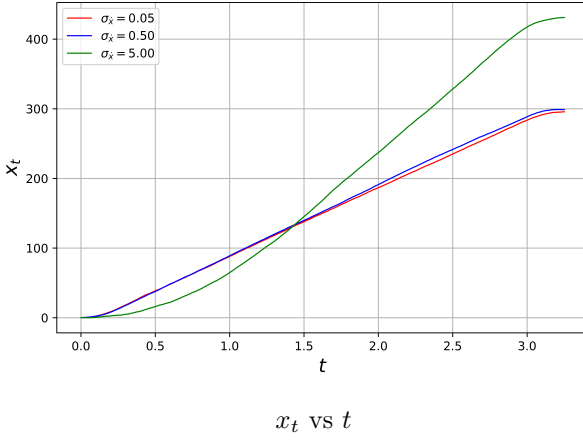


x_t vs t

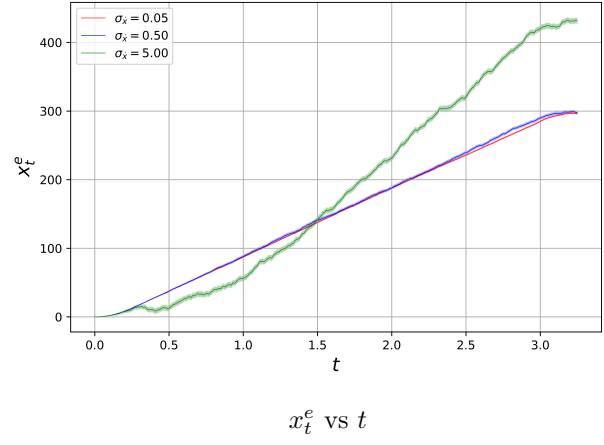


x_t^e vs t

Figure 7: Varying $\sigma_x = 0.01, 0.1, 1.0$

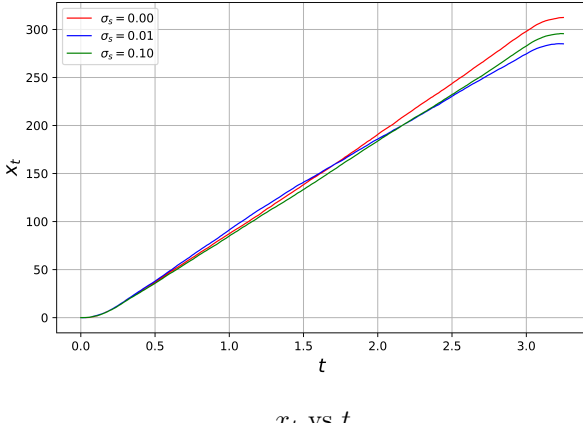


x_t vs t

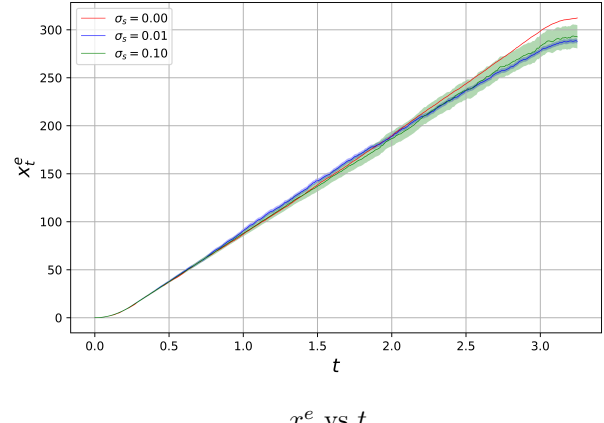


x_t^e vs t

Figure 8: Varying $\sigma_{\dot{x}} = 0.05, 0.5, 5.0$



x_t vs t

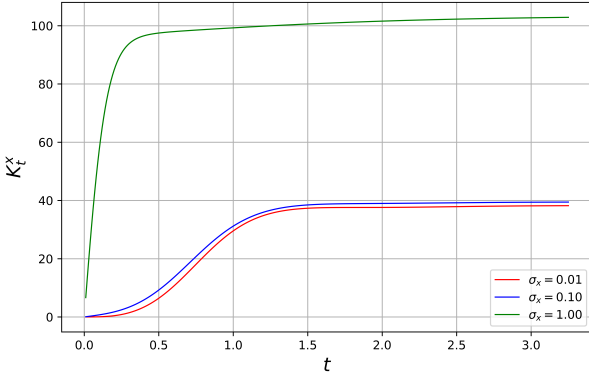


x_t^e vs t

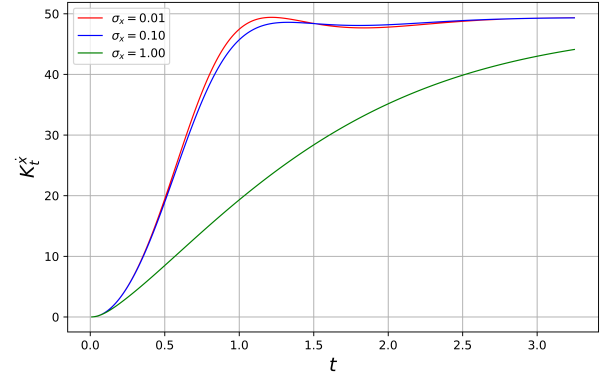
Figure 9: Varying $\sigma_s = 0.001, 0.01, 0.1$

1.5 Kalman Gain

- A larger Kalman Gain implies that we trust the observations more, and update our belief (in the **Update Step**) more strongly as guided by observation, after the **Prediction Step**.
- In [Figure 12](#) we see that reducing σ_s i.e. the expected error in sensor observations, increases both K^x and $K^{\dot{x}}$.
- In [Figure 10](#) and [Figure 11](#) we see as σ_x and $\sigma_{\dot{x}}$ are increased, the Kalman Gain increases. Intuitively, if the model expects the noise in the motion model to be larger, it trusts more on observations.
- In all cases, as time passes, Kalman Gain increases, as the model starts trusting observations more, as the error in motion model keeps getting added.

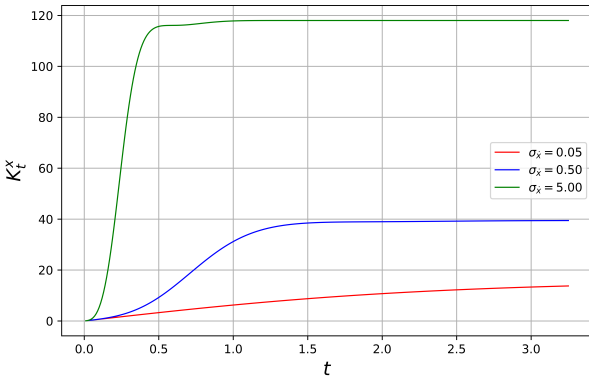


K_t^x vs t



$K_t^{\dot{x}}$ vs t

Figure 10: Varying $\sigma_x = 0.01, 0.1, 1.0$



K_t^x vs t

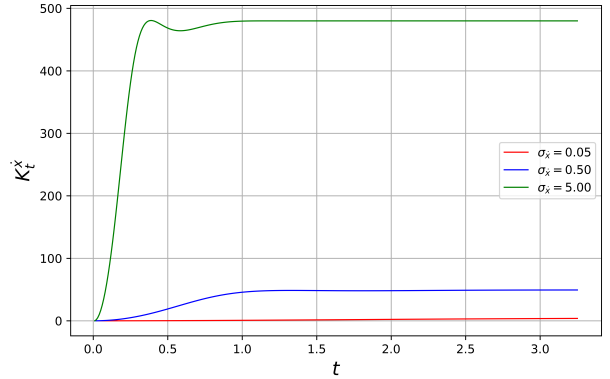
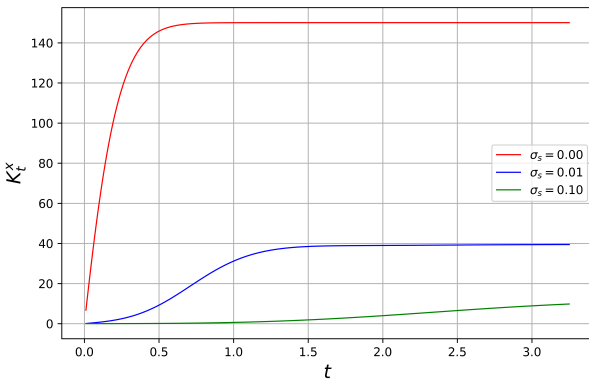


Figure 11: Varying $\sigma_x = 0.05, 0.5, 5.0$



K_t^x vs t

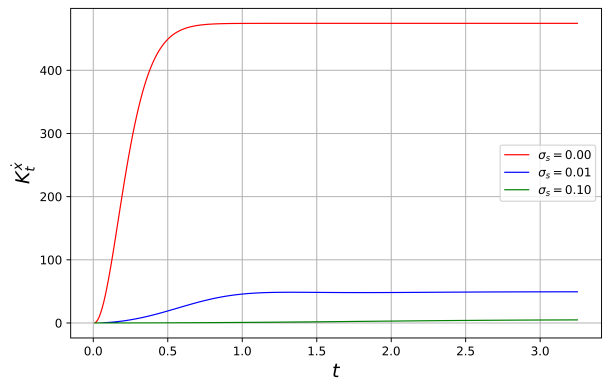


Figure 12: Varying $\sigma_s = 0.001, 0.01, 0.1$

1.6 Missing Observations

In Figure 13, the width of uncertainty bar starts increasing more sharply after $t = 0.5$ (here observations are not available). After $t = 2.5$, the width starts reducing sharply, as observations are now available. The estimated trajectory still ends up very close to the ground truth, as the observations come back later.

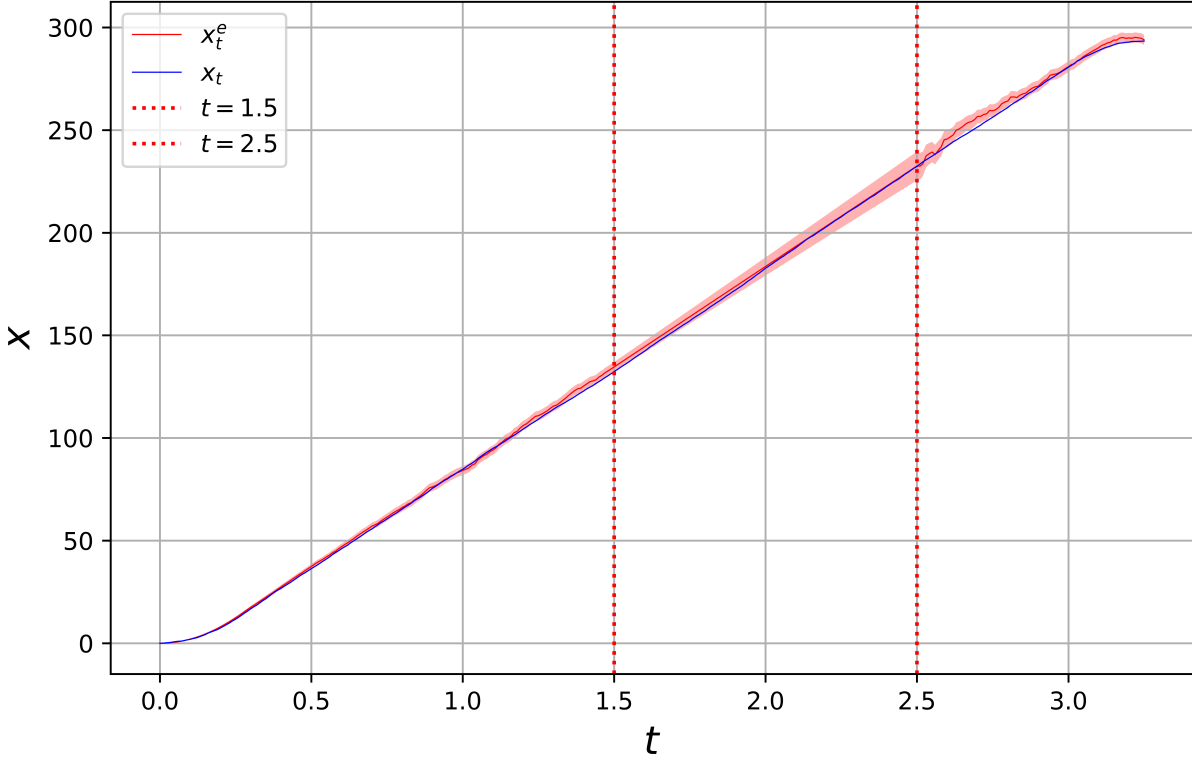


Figure 13: Trajectory x_t^e with missing observations in $t \in [1.5, 2.5]$

2 State Estimation of 3D motion using Kalman Filters

2.1 Motion and Observation models

1. We run the Kalman update after every Δt timestep. The state $X_t \in \mathbb{R}^6$ denotes

$$X_t = \begin{bmatrix} x_t \\ y_t \\ z_t \\ \dot{x}_t \\ \dot{y}_t \\ \dot{z}_t \end{bmatrix}$$

2. The initial belief $X_0 \sim \mathcal{N}(0, 10^{-4}I_6)$ and $u_t = -10$ is a scalar. The motion model is

$$X_{t+1} = A_t X_t + B_t u_t + \epsilon_t$$

$$\text{where } A_t = \begin{bmatrix} I_3 & \Delta t \cdot I_3 \\ O_3 & I_3 \end{bmatrix}, B_t = \begin{bmatrix} 0 \\ 0 \\ \frac{1}{2}\Delta t^2 \\ 0 \\ 0 \\ \Delta t \end{bmatrix}, \epsilon_t \sim \mathcal{N}(0, R_t)$$

$$\text{where } R_t = \text{diag}(\sigma_x^2, \sigma_y^2, \sigma_z^2, \sigma_{\dot{x}}^2, \sigma_{\dot{y}}^2, \sigma_{\dot{z}}^2)$$

3. The observations from IMU sensor are noisy values of ball's position and velocity.
4. The observations from GPS sensor are noisy values of ball's position.
5. The observations from BS sensor are noisy values of ball's distances from $(32, -50, 10), (-32, -50, 10), (-32, 50, 10), (32, 50, 10)$ respectively.
6. See observation models in [Table 1](#).

Sensor	z_t	Z_t	C_t	Q_t
IMU	$[x_t^o \ y_t^o \ z_t^o \ \dot{x}_t^o \ \dot{y}_t^o \ \dot{z}_t^o]^T$	$C_t X_t + \delta_t$	I_6	$\sigma_{IMU}^2 \cdot I_6$
GPS	$[x_t^o \ y_t^o \ z_t^o]^T$	$C_t X_t + \delta_t$	$[I_3 \ O_3]$	$\sigma_{GPS}^2 \cdot I_3$
BS	$[D_1^o \ D_2^o \ D_3^o \ D_4^o]^T$	$h(X_t) + \delta_t$	$J_h(\bar{\mu}_t)$	$\sigma_{BS}^2 \cdot I_4$

Table 1: Observation model parameters for sensors. Here $\delta_t \sim \mathcal{N}(0, Q_t)$

Where

$$h([x \ y \ z \ \dot{x} \ \dot{y} \ \dot{z}]^T) = \begin{bmatrix} \sqrt{(x - a_1)^2 + (y - b_1)^2 + (z - c_1)^2} \\ \sqrt{(x - a_2)^2 + (y - b_2)^2 + (z - c_2)^2} \\ \sqrt{(x - a_3)^2 + (y - b_3)^2 + (z - c_3)^2} \\ \sqrt{(x - a_4)^2 + (y - b_4)^2 + (z - c_4)^2} \end{bmatrix} = \begin{bmatrix} d_1 \\ d_2 \\ d_3 \\ d_4 \end{bmatrix}$$

$$J_h([x \ y \ z \ \dot{x} \ \dot{y} \ \dot{z}]^T) = \begin{bmatrix} \frac{x-a_1}{d_1} & \frac{y-b_1}{d_1} & \frac{z-c_1}{d_1} & 0 & 0 & 0 \\ \frac{x-a_2}{d_2} & \frac{y-b_2}{d_2} & \frac{z-c_2}{d_2} & 0 & 0 & 0 \\ \frac{x-a_3}{d_3} & \frac{y-b_3}{d_3} & \frac{z-c_3}{d_3} & 0 & 0 & 0 \\ \frac{x-a_4}{d_4} & \frac{y-b_4}{d_4} & \frac{z-c_4}{d_4} & 0 & 0 & 0 \end{bmatrix}$$

2.2 Kalman Filter Model

In all three cases, the trajectory is very close to the Ground Truth strategy, except for small fluctuations, there are no visible deviations. For IMU and GPS sensors, we use Kalman model given in [Figure 5](#) using values in [Table 1](#). The observation of BS sensor is a non-linear function of X_t so we use EKF Linearization, given in [Figure 14](#).

Algorithm Kalman_filter_EKF($\mu_{t-1}, \Sigma_{t-1}, u_t, z_t$)

Prediction Step

$$\bar{\mu}_t = A_t \mu_{t-1} + B_t u_t$$

$$\bar{\Sigma}_t = A_t \Sigma_{t-1} A_t^T + R_t$$

Update Step

$$K_t = \bar{\Sigma}_t J_h(\bar{\mu}_t)^T (J_h(\bar{\mu}_t) \bar{\Sigma}_t J_h(\bar{\mu}_t)^T + Q_t)^{-1}$$

$$\mu_t = \bar{\mu}_t + K_t(z_t - h(\bar{\mu}_t))$$

$$\Sigma_t = (I - K_t J_h(\bar{\mu}_t)) \bar{\Sigma}_t$$

return μ_t, Σ_t

Figure 14: Kalman Filter Algorithm with EKF Linearization

2.3 Automated Referee

1. I increased the number of time-steps to 150, keeping Δt same to ensure every trajectory passes through the goal plane $y = 50$. The decision for goal is that, if ball's coordinates are $(x, 50, z)$ then $-4 < x < 4$ and $0 < z < 3$.
2. Since sensor readings and filter outputs are at discrete time-steps, we may not have positions when ball is exactly in the $y = 50$ plane. So we interpolate linearly.
3. In case of Ground Truth, we search through the trajectory to find, if any (x_t, y_t, z_t) and $(x_{t+1}, y_{t+1}, z_{t+1})$ such that $y_t \leq 50.0 \leq y_{t+1}$. Then we linearly interpolate to get x, z approximately at $y = 50$. The same is done for GPS, but the trajectory is purely the GPS observations.
4. When using filter outputs, we do the same interpolation with (μ_t, μ_{t+1}) and covariance matrices (Σ_t, Σ_{t+1}) . Then we take the (x, z) sub-matrix to get the approximate distribution of (x, z) at $y = 50$. Then we find the fraction of the volume of Gaussian's volume in $-4 < x < 4$ and $0 < z < 3$. This gives probability of a goal. This is compared to a threshold to get the decision. The volume computation is simple because the covariance matrix of (x, y, z) here is always diagonal due to the specific values in motion and observation model.

2.4 Varying noise parameters in Automated Referee

- The output in [Table 2](#) was generated by keeping threshold 0.8. Number of goals in case of Filter are in same order, but lesser than that of Ground Truth and Raw observations, possibly due to high threshold.
- Case of the default parameters, the number of goals is nearly $\frac{1}{4}^{th}$. Consider a Gaussian centered at the corner. The goal has roughly one fourth of area covered, assuming density is very small far from the corner.

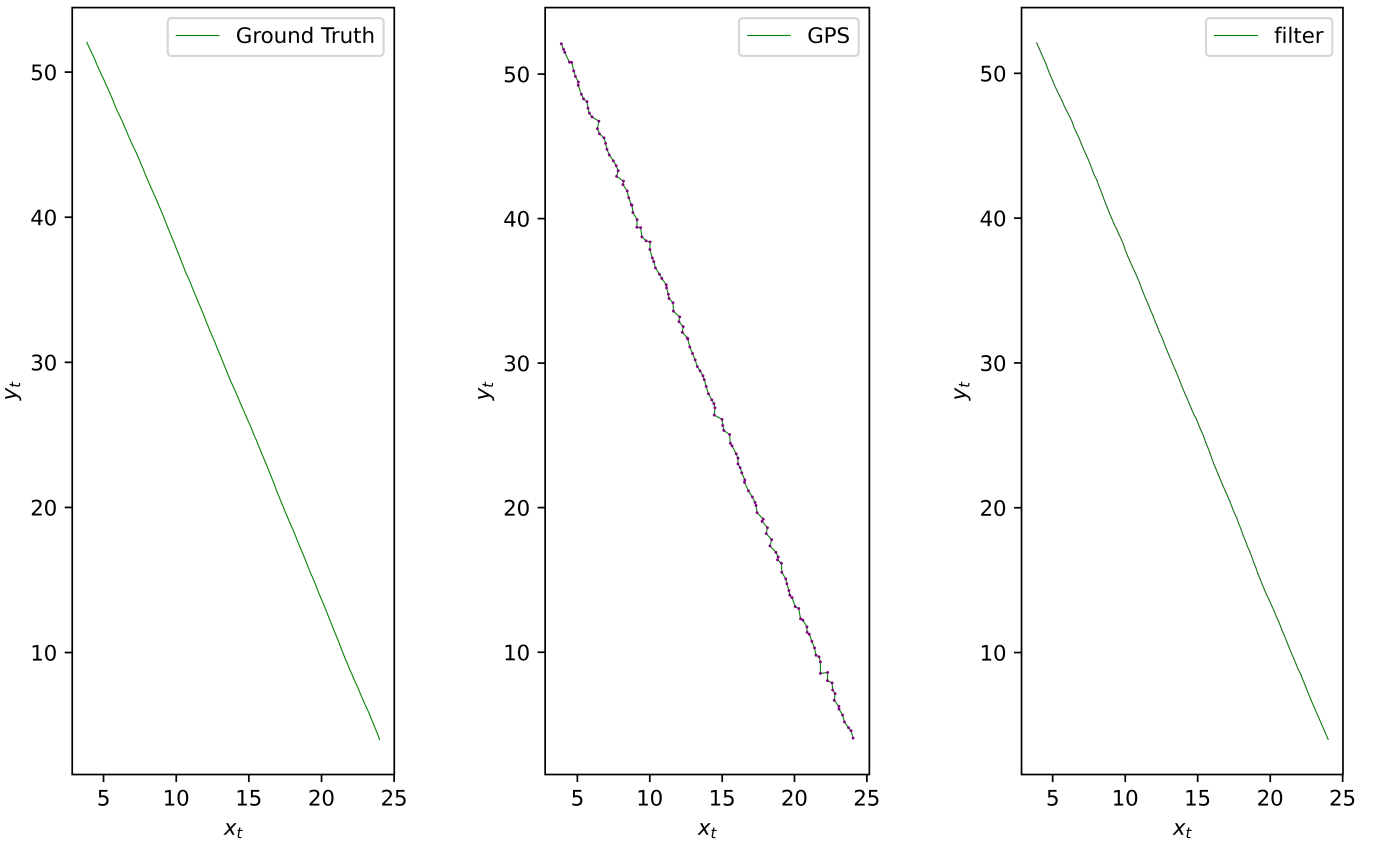
- The Filter produces particularly low values, when one of the three noise parameters is very high, likely because more density distributed away from the corner (high $\sigma_{observation}$), or larger deviations in trajectory (high $\sigma_x, \sigma_{\dot{x}}$).

$\sigma_x, \sigma_y, \sigma_z$	$\sigma_{\dot{x}}, \sigma_{\dot{y}}, \sigma_{\dot{z}}$	σ_{BS}	Ground Truth	IMU	Filter _{IMU}	GPS	Filter _{GPS}
0.0010	0.0100	0.0100	534	443	477	526	507
0.0010	0.0100	0.1000	534	451	481	439	414
0.0010	0.0100	1.0000	501	426	446	182	33
0.0010	0.1000	0.0100	246	235	242	246	245
0.0010	0.1000	0.1000	274	265	271	275	262
0.0010	0.1000	1.0000	247	238	245	201	173
0.0010	1.0000	0.0100	27	27	27	27	27
0.0010	1.0000	0.1000	29	28	29	30	28
0.0010	1.0000	1.0000	33	32	33	29	21
0.0100	0.0100	0.0100	389	376	297	390	368
0.0100	0.0100	0.1000	409	410	334	403	327
0.0100	0.0100	1.0000	391	366	316	191	55
0.0100	0.1000	0.0100	281	278	265	278	275
0.0100	0.1000	0.1000	252	257	245	250	238
0.0100	0.1000	1.0000	293	294	275	212	207
0.0100	1.0000	0.0100	37	35	37	37	37
0.0100	1.0000	0.1000	27	27	27	27	26
0.0100	1.0000	1.0000	33	34	32	35	23
0.1000	0.0100	0.0100	205	207	185	203	199
0.1000	0.0100	0.1000	208	212	188	213	194
0.1000	0.0100	1.0000	212	219	200	211	142
0.1000	0.1000	0.0100	165	167	152	166	164
0.1000	0.1000	0.1000	207	207	195	213	197
0.1000	0.1000	1.0000	192	194	176	154	129
0.1000	1.0000	0.0100	20	21	18	21	21
0.1000	1.0000	0.1000	31	30	29	30	30
0.1000	1.0000	1.0000	31	29	29	31	18

Table 2: Goal detection results for different parameter values.

2.5 Uncertainty Ellipses on Trajectory

- See [Figure 15](#) (zoom it to see the ellipses). In case of GPS observations, these are indeed circles, as Q_t is diagonal with same entry in x and y . We see all these circles have the same radius, as Q_t remains same.
- In case of Filter outputs, the circles start very small in the start but increase in size later. These are indeed circles as in output of Kalman Filter, the sub-matrix of (x, y, z) is diagonal. Uncertainty is lesser than the previous case as here we incorporate both, actions and observations.



Ground Truth trajectory

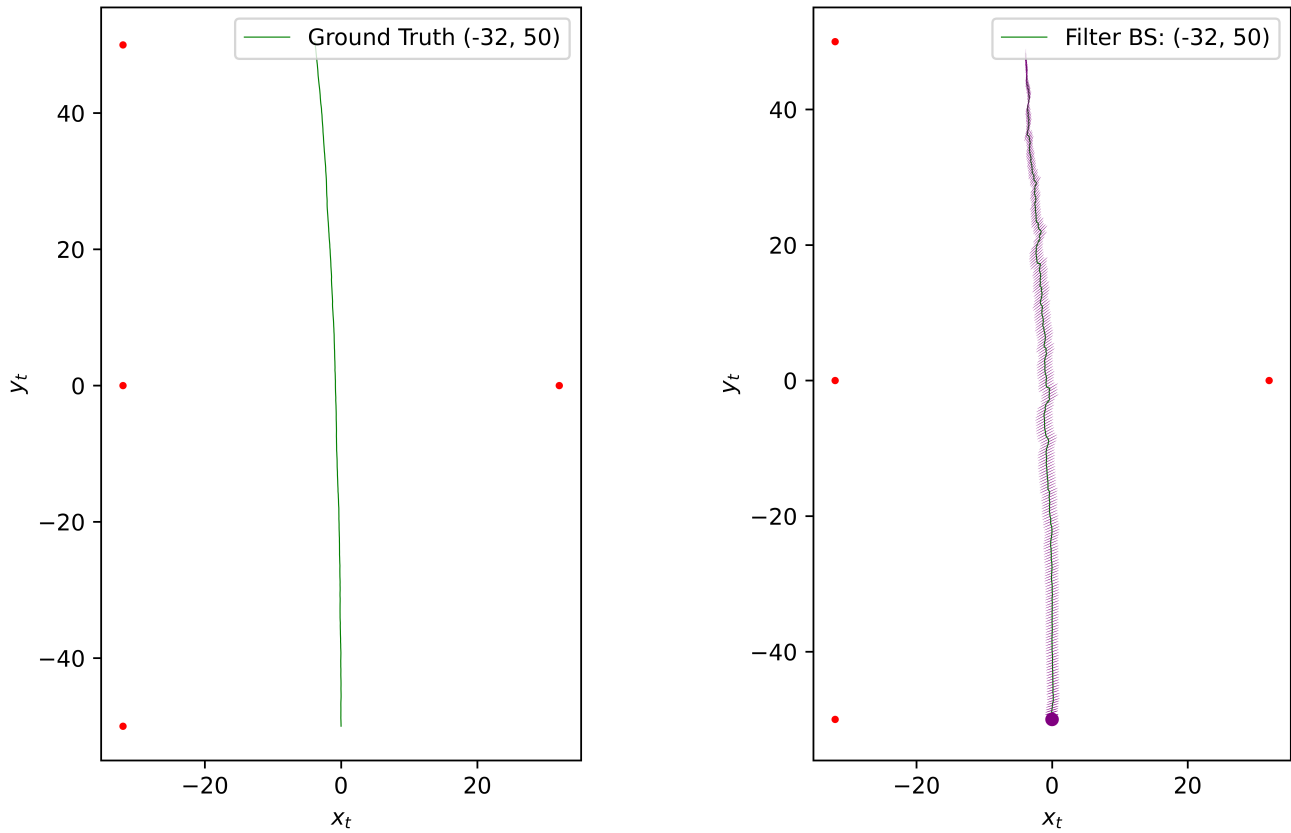
Trajectory using GPS observations

Trajectory output by Kalman Filter

Figure 15: Uncertainty ellipses

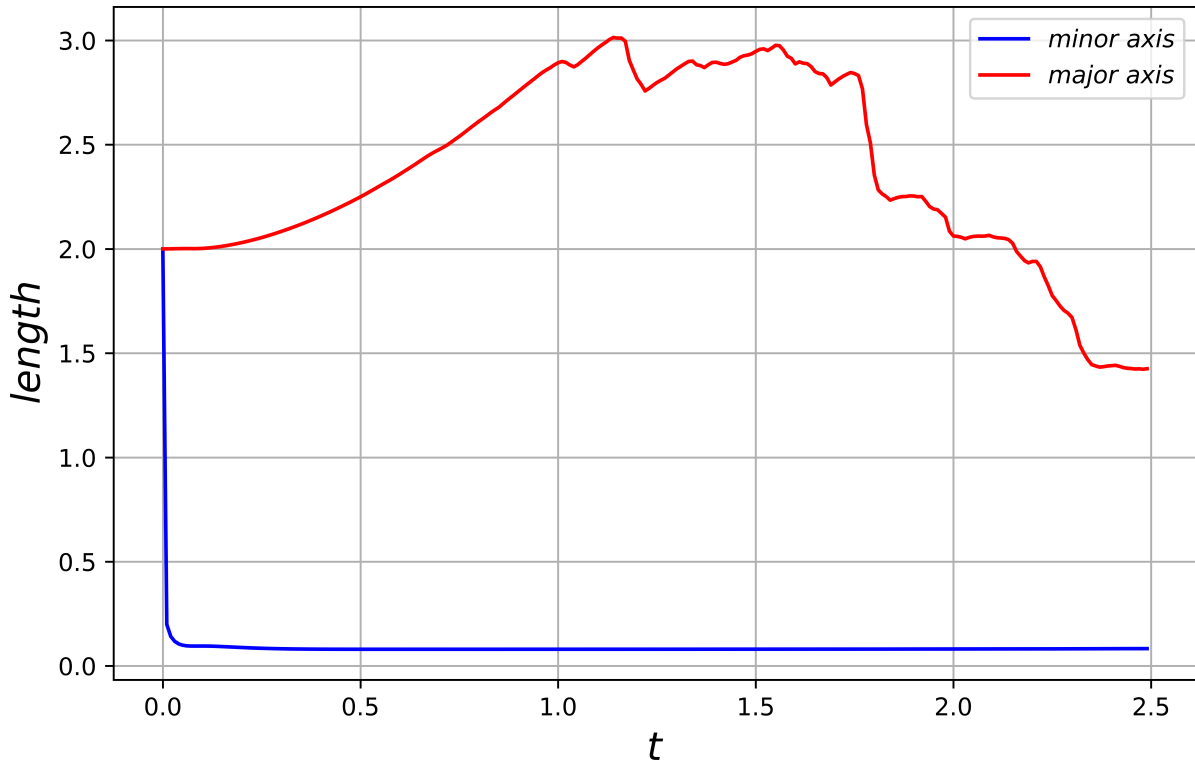
2.6 Base-Stations in 2D Kinematics

1. In case of single BS sensors, for any point on the trajectory, the minor axis of the corresponding uncertainty ellipse is nearly in direction of that line joining the BS sensor to that point on the trajectory.
2. Let the BS be at origin and the vector from BS sensor to point on trajectory be \vec{d} . For the same small step size α , movement also \vec{d} changes sensor observation by larger amount ($= \alpha$) compared to moving perpendicular to \vec{d} ($= \sqrt{d^2 + \alpha^2} - d$). Hence, given sensor observation, if actual value deviates along \vec{d} , it is likely deviates less, as the distance increases rapidly in this direction, while the range $[x^e - \sigma_{x^e}, x^e + \sigma_{x^e}]$ is fixed.
3. The minor axis falls sharply in all cases. The major axis seems to have a minimum when the point is closest to the sensor.



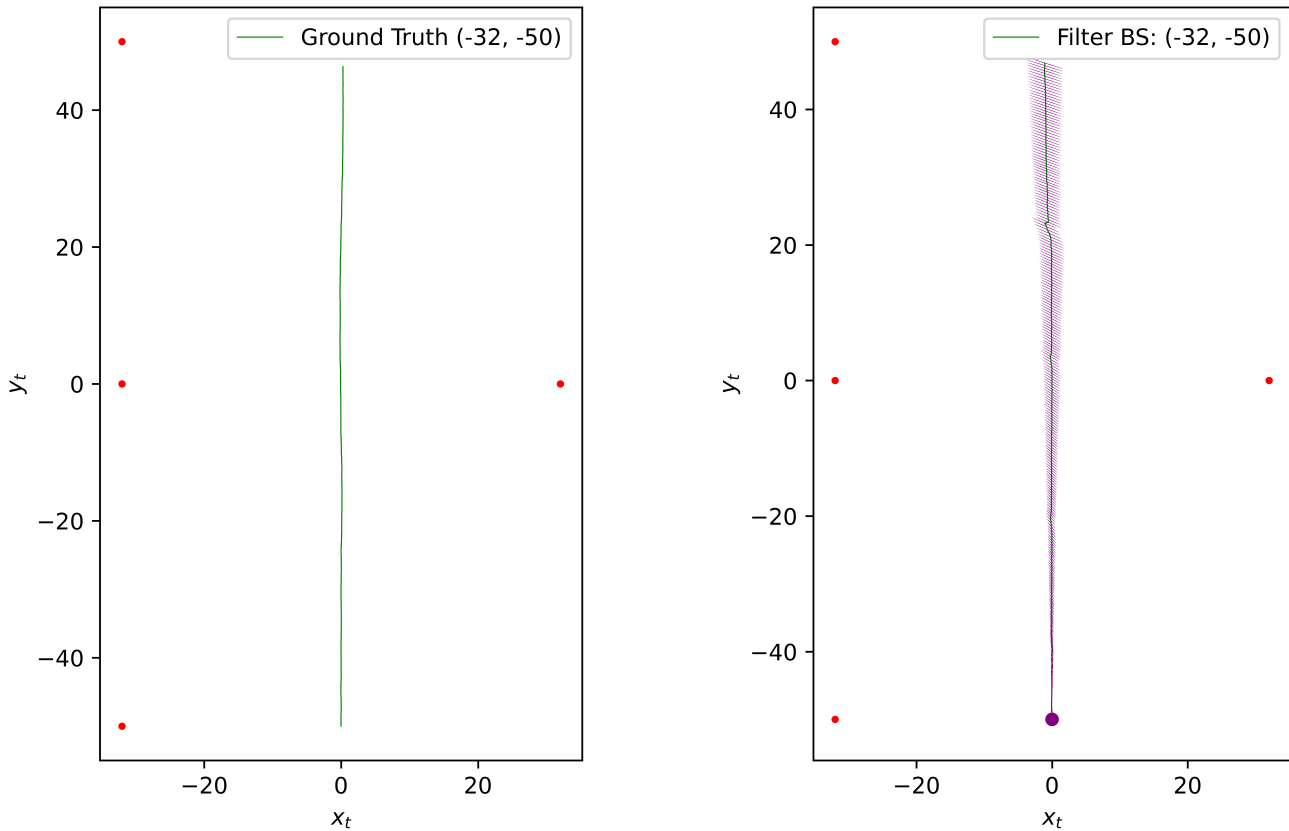
Ground Truth

Kalman Filter



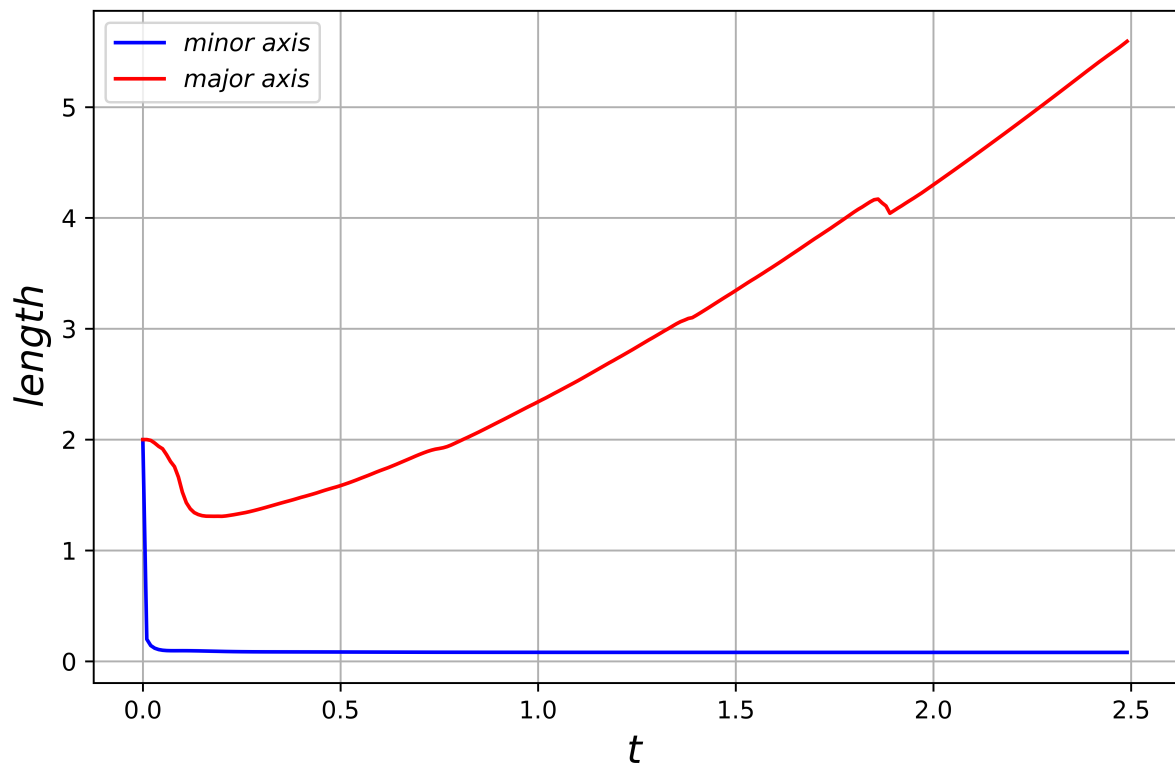
Major and Minor Axes

Figure 16: Base-Station $B_1(-32, 50)$



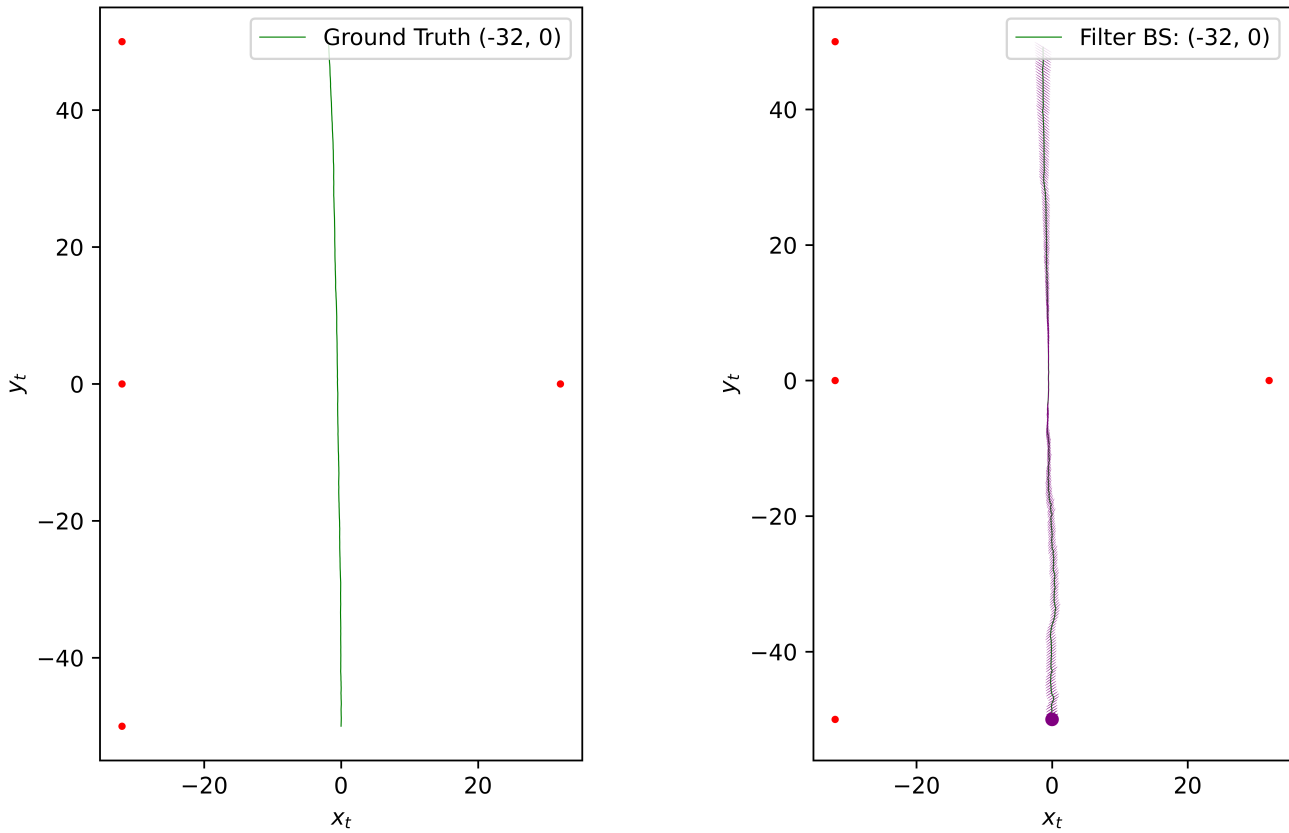
Ground Truth

Kalman Filter



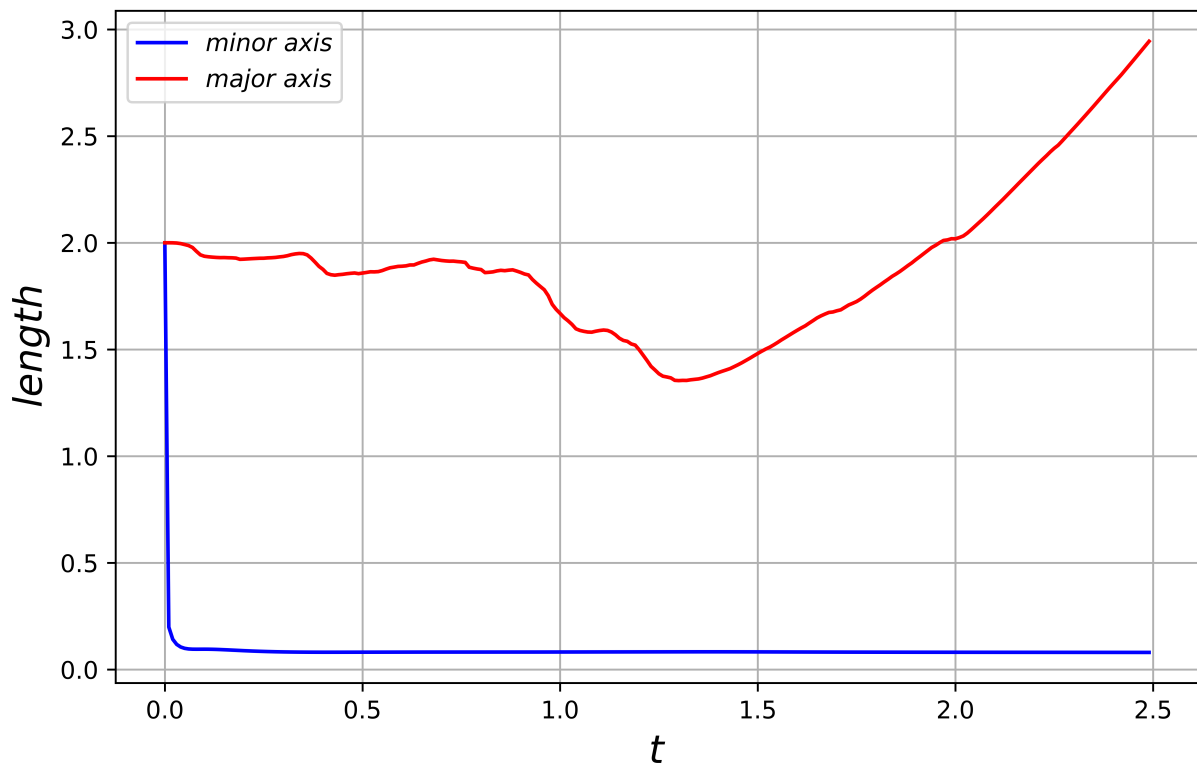
Major and Minor Axes

Figure 17: Base-Station $B_2(-32, -50)$



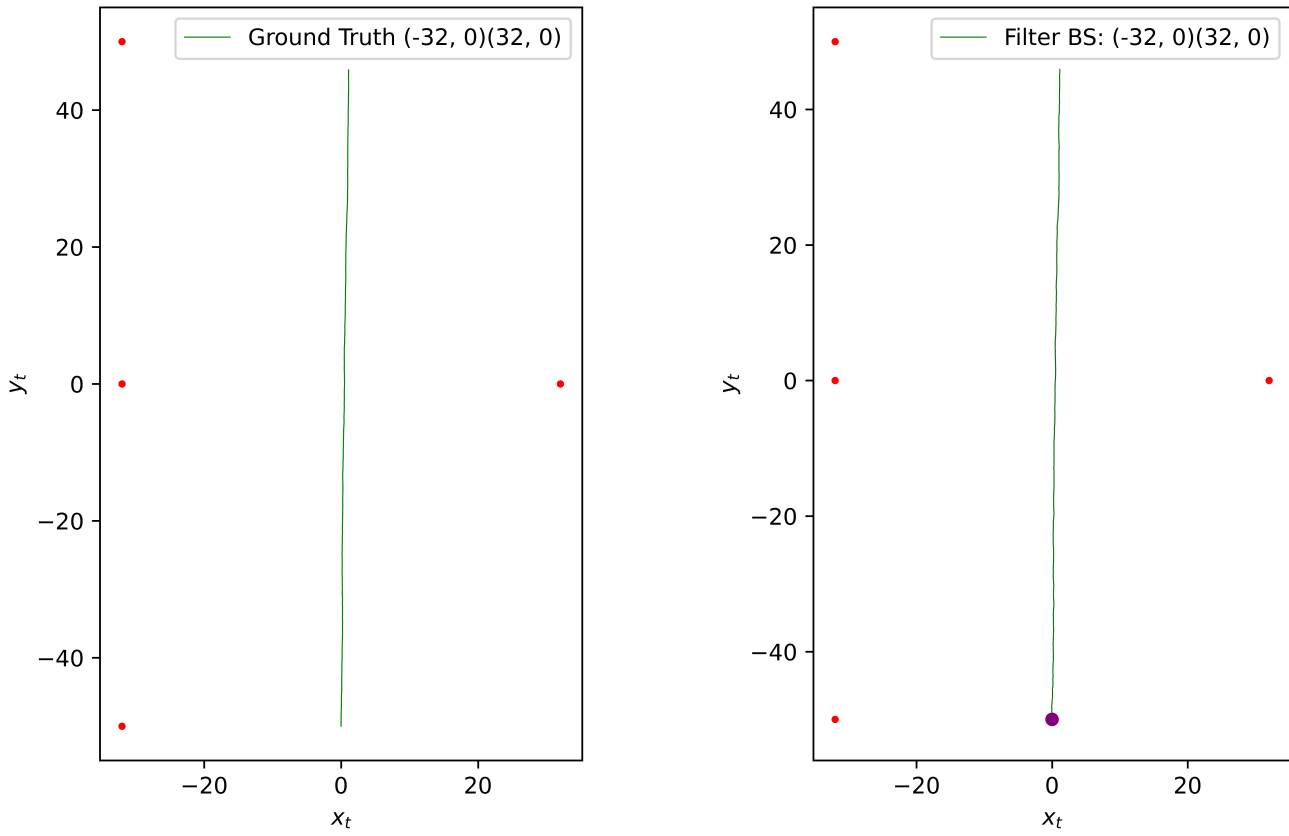
Ground Truth

Kalman Filter



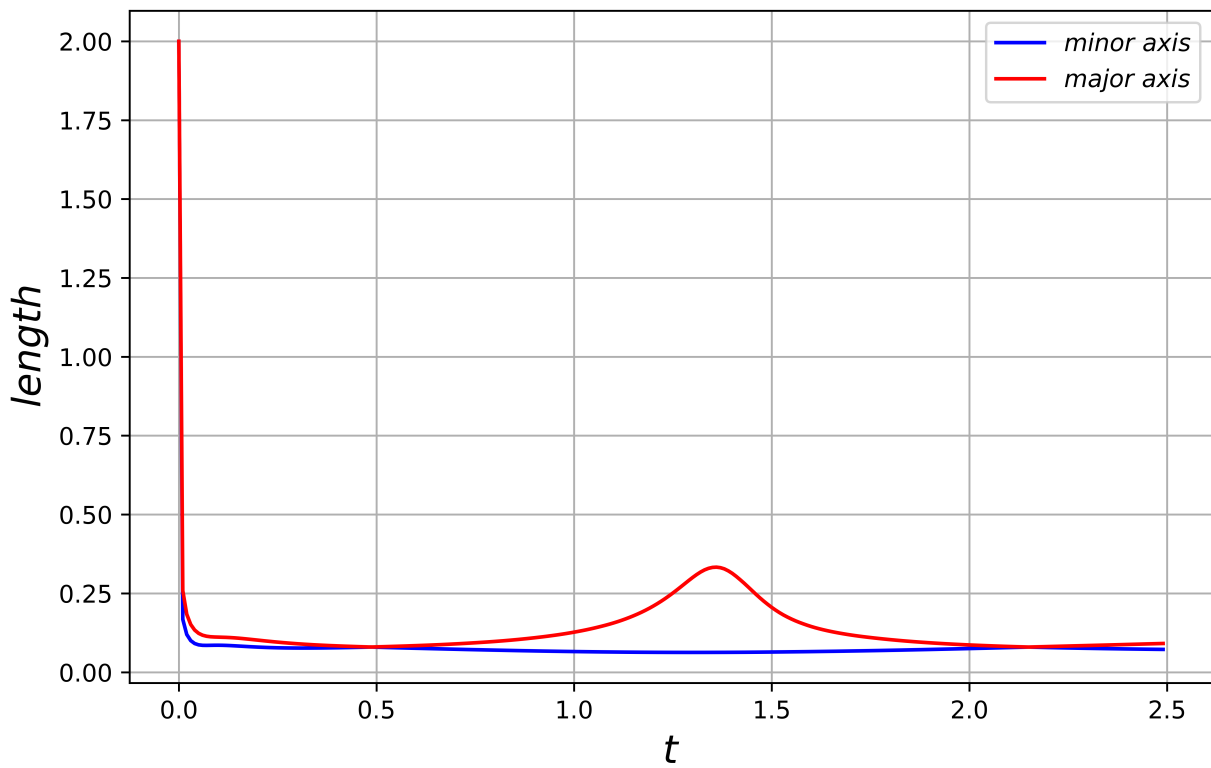
Major and Minor Axes

Figure 18: Base-Station $B_3(-32, 0)$



Ground Truth

Kalman Filter



Major and Minor Axes

Figure 19: Base-Station $B_3(-32, 0), B_4(32, 0)$

3 More insights after viva

1. See [Figure 6](#). We see that initially, the uncertainty bar is very narrow, then it becomes broader and remains more or less constant. This is because our initial belief is very narrow, $\Sigma_0 = 10^{-4}I_2$. σ_x starts with 0.01 and finally becomes ≈ 2.44 , increasing very slowly in later time steps. This happens because the error in the motion model keeps accumulating, but it does not increase much beyond a point, as the observations keep making the belief tighter. On the contrary, see [Figure 18](#), where the initial belief has large variance.
2. Consider the setup in a 1D kinematics problem. See [Figure 5](#), if $\bar{\Sigma}_t = \begin{bmatrix} \alpha_x^2 & \rho\alpha_x\alpha_{\dot{x}} \\ \rho\alpha_x\alpha_{\dot{x}} & \alpha_{\dot{x}}^2 \end{bmatrix}$, then assuming $C_t = [1 \ 0]$, the Kalman Gain is $K_t = \frac{1}{\alpha_x^2 + \sigma_s^2} \begin{bmatrix} \alpha_x^2 \\ \rho\alpha_x\alpha_{\dot{x}} \end{bmatrix}$. We see that the belief in velocity gains from the observation only if the model sees that there's a correlation between velocity and position. The correlation is inferred from the action model. Again, in [Figure 5](#), if $\Sigma_{t-1} = \alpha I$, then $A_t \Sigma_{t-1} A_t^T = \alpha \begin{bmatrix} 1 + \Delta t^2 & \Delta t \\ \Delta t & 1 \end{bmatrix}$. This fundamentally happens because x_t is affected by v_{t-1} .
3. If we have IMU and GPS sensors with the same $\sigma_x, \sigma_y, \sigma_z$ in both, irrespective of $\sigma_{\dot{x}}, \sigma_{\dot{y}}, \sigma_{\dot{z}}$, the IMU sensor will always perform better than the GPS sensor in expectation. The information about x, y, z provided by both of them is similar. If $\sigma_{\dot{x}}, \sigma_{\dot{y}}, \sigma_{\dot{z}}$ are very low, the IMU will clearly provide more information. Even if they are very high, the Kalman Filter will itself decrease the Kalman Gain from the velocity observations, as their variance is known. In the limit, for example, when the variance in velocity observation is infinite, the Kalman Gain for velocity observation will be zero.
4. If there were no error in the motion model, the ball would hit the goal at $t = 1.25$ seconds, at $(3.95, 50, 2.95)$, which is very close to the corner of the goal.
5. It can be proved using induction that in the case of IMU and GPS sensors, $\Sigma_t = \begin{bmatrix} aI_3 & bI_3 \\ bI_3 & cI_3 \end{bmatrix}$. Hence, in [Figure 15](#), all ellipses in the filter output are perfect circles. This is due to the particular forms of A_t, R_t, C_t, Q_t in our setup.
6. We now know that a BS sensor has **poor information** in the tangential direction. In [Figure 18](#), notice the dip in the length of the major axis. At this point, the **new information** in the radial direction reduces the uncertainty that was present when the particle started (here, the tangential direction has a positive cosine with the radial direction at the point of dip).
7. The Kalman Filter outputs Σ_t . To analyze the uncertainty in lower dimensions, it is only correct to project the motion onto the xy-plane, as in [Figure 18](#), since all covariance terms are 0. When this is not the case, for example, when using the BS sensors, the projection should be along the plane of eigen-directions. In simpler terms, the diagonal entries do not indicate uncertainty as well as the eigenvalues do, but this will be along the eigen-directions.